

# 1       **Terrestrial heat flow evaluation from thermal response tests** 2                               **combined with temperature profiling**

3

4   Maria Isabel Velez<sup>1</sup>, Jasmin Raymond<sup>1</sup>, Daniela Blessent<sup>2</sup>, Mikael Philippe<sup>3</sup>

5   <sup>1</sup> Centre Eau Terre Environnement, Institut national de la recherche scientifique, 490 rue de la  
6   couronne, Québec (Qc), Canada.

7   <sup>2</sup> Programa de Ingeniería Ambiental, Universidad de Medellín, Carrera 87 N° 30 – 65, Medellín,  
8   Colombia.

9   <sup>3</sup> Georesources Division, BRGM, 3 avenue Claude Guillemin, BP 36009, 45060 Orléans Cedex 2,  
10   France.

11   **Key words:** Geothermal, Heat flow, Thermal response test, Paleoclimate, Temperature  
12   profile, Thermal conductivity.

13

## 14   **ABSTRACT**

15   The terrestrial heat flux density, an essential information to evaluate the deep  
16   geothermal resource potential, is rarely defined over urban areas where energy needs  
17   are important. In an effort to fill this gap, the subsurface thermal conductivity estimated  
18   during two thermal response tests was coupled with undisturbed temperature profile  
19   measurements conducted in the same boreholes to infer terrestrial heat flow near the  
20   surface. The undisturbed temperature profiles were reproduced with an inverse  
21   numerical model of conductive heat transfer, where the optimization of the model bottom  
22   boundary condition allows determining the near-surface heat flow. The inverse numerical  
23   simulation approach was previously validated by optimizing a steady-state and synthetic  
24   temperature profile calculated with Fourier's Law. Data from two thermal response tests  
25   in ground heat exchangers of one hundred meters depth were analyzed with inverse  
26   numerical simulations provided as examples for the town of Québec City, Canada, and  
27   Orléans, France. The temperature profiles measured at the sites and corrected  
28   according to the paleoclimate effects of the quaternary glaciations were reproduced with  
29   the model. The approach presented offers an alternative to assess heat flow in the  
30   preliminary exploration of deep geothermal resources of urban areas, where thermal  
31   response tests may be common while deep wells sparsely distributed over the area to  
32   assess heat flow.

## 33        1 Introduction

34    Heat flow is the main source of information about the Earth's thermal state (Golovanova  
35    *et al.*, 2014). Nevertheless, measuring the Earth's heat flow is difficult and only sparse  
36    data are available, especially in urban areas. Terrestrial heat flow is estimated by  
37    combining temperature profile and thermal conductivity data sets from deep boreholes  
38    (Bodri & Cermak, 2007; Sass & Beardsmore, 2011), typically more than 300 m depth  
39    (Jessop, 1990; Beck, 1977). The temperature gradient is derived from point  
40    measurements of temperature at two or more discrete depths and thermal conductivity is  
41    commonly evaluated on core samples at the surface, either in the field or in the  
42    laboratory. As exploratory drilling for petroleum and minerals became widespread,  
43    temperature profiles measured in boreholes became the most common means of  
44    determining temperature gradients within the Earth (Sass & Beardsmore, 2011). This  
45    information has been analyzed to estimate local heat flow values and produce regional  
46    maps. Such interpolation of heat flow estimates has since been carried out worldwide as  
47    a tool to better understand the thermal structure of the near surface that plays a role in  
48    the exploration of hydrocarbons, geothermal and mineral resources (Davies, 2013). The  
49    information given on heat flow map is particularly useful for the exploration of geothermal  
50    resources. However, deep mineral or hydrocarbon exploration wells to measure  
51    temperature are almost inexistent in urban areas where energy needs are important.

52    This created a data gap evidencing the needs to adapt methods to assess heat flow over  
53    urban areas at the early stage of geothermal exploration projects before pursuing deep  
54    drilling.

55    For example, the heat flow map of Eastern Canada has been built analyzing available  
56    heat flow data for the Canadian Shield and the Appalachians. There are actually more  
57    than 300 reliable heat flow values in the Canadian Shield, including 150 heat flow  
58    evaluations around Lake Superior, with boreholes usually deeper than 100 m (Mareschal  
59    & Jaupart, 2004). Nevertheless, none of the locations with heat flow assessments are  
60    located over urban areas such as Quebec City, Montreal or Toronto with significant  
61    energy demand. The heat flow map of France was inferred interpolating 479 heat flow  
62    assessments inside the country combined with additional data from Spain, Switzerland,  
63    German and Italy (SIG Mines France, 2007). Again, heat flow assessments over cities  
64    are rare, although they can be more common in Europe than North-East America. In

fact, heat flow observations are non-uniformly distributed (Davies, 2013) and information is far from being completed in urban areas. Nevertheless, the development of geothermal heat pump systems, taking place in populated cities, is creating opportunities to estimate heat flow from subsurface thermal conductivity and temperature data, obtained in shallow boreholes.

Thermal response tests (TRT) are commonly used to assess the subsurface thermal conductivity to design shallow geothermal systems (Raymond & Lamarche, 2014), like ground-coupled heat pumps including boreholes of 100 to 200 m depth. The ground temperature and thermal conductivity estimated during a TRT could be useful to infer the terrestrial heat flow (Sanner *et al.*, 2013), filling data gaps over urban areas. Inverse numerical modeling was previously achieved by Raymond *et al.* (2016) to reproduce temperature profiles measured in ground heat exchangers and estimate heat flow to spatially extend a TRT assessment, which was believed to be useful when designing large ground-coupled heat pumps systems enclosing several heat exchangers. The proposed method could similarly be used to evaluate heat flow through the scope of deep geothermal resource assessment, but needs to be improved by taking into account surface temperature changes as climate warming can significantly affect temperature profile measured in shallow ground heat exchangers.

Heat flow estimations, based on depth-temperature measurements, generally require corrections for paleoclimate effects (Westaway & Younger, 2013). Paleoclimate correction account for temperature changes at the Earth's surface that slowly propagates downward into the subsurface and appear as tiny temperature deviations imposed on the geothermal gradient (Bodri & Cermak, 2007). The past variations in surface temperature relative to its present value can be approximated as a series of step changes, each starting at a particular time before the present day to correct temperature profiles. This is especially important for shallow boreholes affected by ground surface temperature variations. The objective of this work was to estimate the heat flow near the surface combining TRT field data with undisturbed temperature profile and historic atmospheric temperature measurements, which evaluate the recent surface warming. TRTs allows estimating thermal conductivity at different depths to define thermostratigraphic layers and reduce the assumptions made with punctual laboratory measurements on rock samples. TRT data are becoming relatively abundant in urban regions, where shallow geothermal heat pump systems are now installed. The

hypothesis studied is that thermal conductivity data provided by TRT in shallow boreholes of 100 to 200 m depth could be useful to estimate heat flow near the Earth surface, provided that undisturbed temperature profiles can be measured and analyzed at the same location. Such estimation can complement sparse heat flow assessment from deeper wells typically located outside urban areas, assuming that the effect of climate warming can be adequately considered when modeling the temperature profiles of shallow boreholes. Thermal conductivity profiles estimated during TRT with heating cables at two experimental sites in Canada and France were used to build an inverse transient heat transfer 1D model with the finite element method implemented in COMSOL Multiphysics (COMSOL AB). The sites are experimental research platforms with ground heat exchangers and available thermal conductivity data sets from thermal response tests conducted in the past. The optimization of the model bottom boundary condition to reproduce the undisturbed temperature profiles measured in the boreholes, taking into account historic temperature measurement at the surface, allowed estimating the Earth heat flow in the two cities.

## 2 Methodology

In situ thermal conductivity evaluated at depth during the two TRTs performed with heating cables were used as inputs to define the numerical model properties. Inverse transient heat transfer simulations were carried out with COMSOL Multiphysics to reproduce the undisturbed temperature profiles measured in the ground heat exchangers before the TRT.

### 2.1 *In situ* thermal conductivity assessment

The first TRT was carried out in an experimental borehole of approximately 100 m depth at the Laboratoires for scientific and technological innovation in environment (LISTE) of the Institut national de la recherche scientifique, located in Quebec City, Canada (Experimental site 1). The test was performed using heating cable sections and the finite line source solution was used to reproduce the temperature evolution along the heating section and estimated the thermal conductivity. The second TRT was completed at the experimental geothermal test facility of the French geological survey (Bureau de Recherches Géologiques et Minières) in Orléans, France (Experimental site 2), with a

continuous heating cable. This test was analyzed using the infinite line source solution (Velez *et al.*, 2018).

The equipment required to perform the tests consists of a heating cable, a junction box to link the cable to the power supply and submersible sensors to measure and record the temperature during the tests (Velez *et al.*, 2018). In Quebec City, the thermal conductivity was evaluated every 10 m and allowed to define 10 thermal conductivity layers in the model domain. The estimated thermal conductivity ranged between 1.72 to 2.19  $\text{W m}^{-1}\text{K}^{-1}$ , with an average value of 2.02  $\text{W m}^{-1}\text{K}^{-1}$  (Figure 1). In Orléans, thermal conductivity was assessed every 6 m in a borehole of similar depth allowing to define 13 thermal conductivity layers in the model domain. The thermal conductivity varied from 1.08 to 2.18  $\text{W m}^{-1}\text{K}^{-1}$  with a mean value of 1.47  $\text{W m}^{-1}\text{K}^{-1}$  (Figure 1).

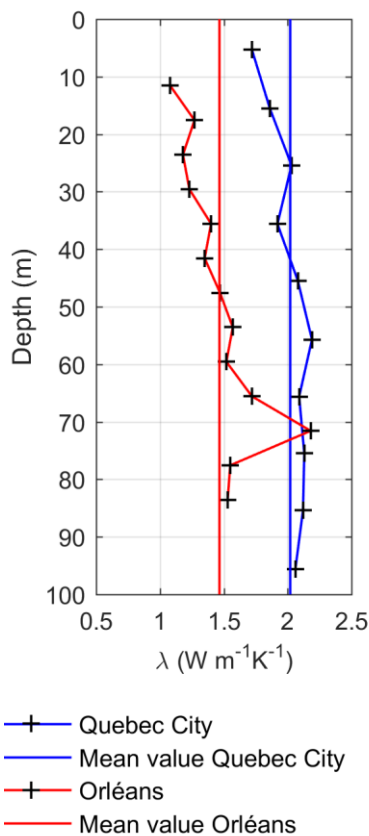


**Figure 1. Thermal conductivity profiles and mean thermal conductivity in Quebec City and Orléans.**

## 2.2 Temperature measurements and paleoclimate correction

The temperature profile at experimental site 1 was measured using a submersible temperature and pressure data logger (RBRduet) with an accuracy of 0.002 °C. The logger was attached to a wire and gradually lowered in the borehole achieving a spatial resolution of approximately 2.4 m. The ground heat exchanger in Orléans was equipped with a fiber optic distributed temperature sensing (FO-DTS) system and the temperature profile was measured using the fiber optic cable with a temperature resolution of +/- 0.05 °C and a spatial resolution of 1 m.

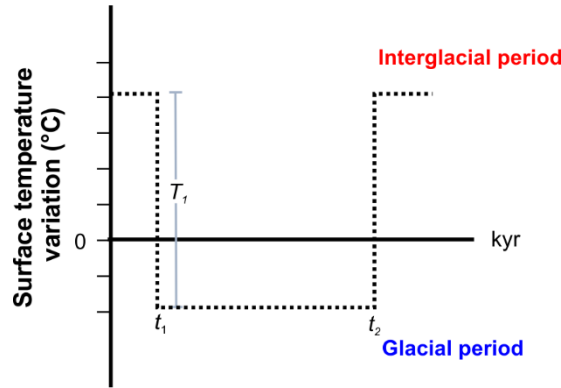


**Figure 2. Example of the surface temperature variation assumed during a glacial period (kyr = thousand years).**

The initial temperature measured in the ground heat exchangers before conducting the TRT was corrected according to the influence of the paleoclimate temperature variations due to the last Quaternary glaciations (Eq. 1). The correction is computed at each depth  $z$  (m), and depends on the duration of the glacial periods ( $t_1$ ,  $t_2$ ; Figure 2), the temperature drop with respect to the present surface average temperature ( $T_1$ ; Figure 2) and the thermal diffusivity of the rocks (Jessop, 1990). The corrected temperature is

$$T_c = T_m - \sum_i (T_{i_1}) \cdot \left[ \operatorname{erf} \left( \frac{z}{2\sqrt{\alpha_s t_{i_1}}} \right) - \operatorname{erf} \left( \frac{z}{2\sqrt{\alpha_s t_{i_2}}} \right) \right] \quad (1)$$

where  $T_m$  (K) is the temperature measured at each depth and  $\alpha_s$  ( $\text{m}^2 \text{s}^{-1}$ ) is the thermal diffusivity.

The last four glaciations in North America were considered for paleoclimate corrections at experimental site 1 (Figure 3). The temperature during the interglacial periods was assumed as the present day mean annual ground temperature (Allis, 1978, Jessop,

1990) and a temperature step of 5 K was supposed (Jessop, 1990). The last five glaciations in Europe and a temperature amplitude of 7 K were assumed for the experimental site 2 (Figure 4), according to the surface temperature history and a temperature step of 7 K proposed by Majorowicz and Šafanda (2008) and Majorowicz and Wybraniec (2011).

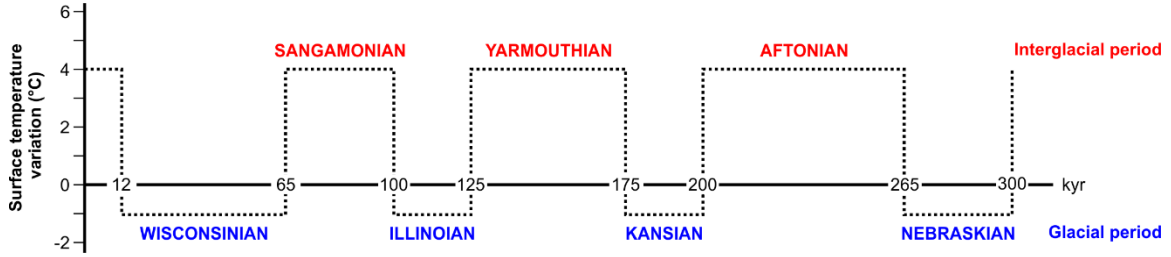


**Figure 3. Chronology of glacial periods in Canada considered at the experimental site 1 in Quebec City (modified from Bédard *et al*, 2017, kyr = thousand years).**

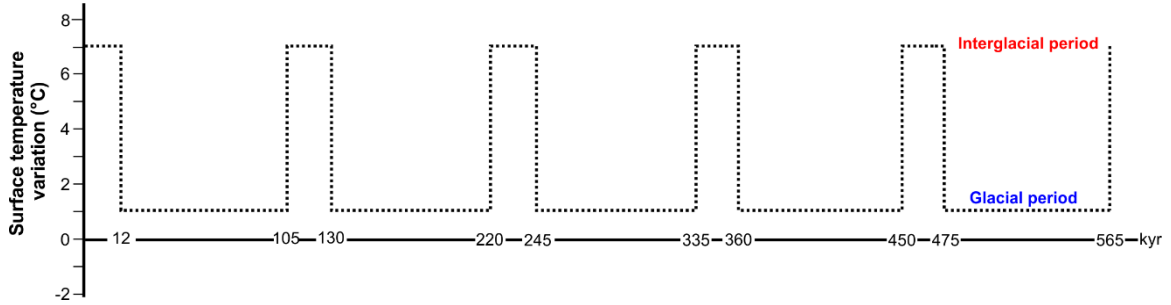


**Figure 4. Chronology of glacial periods in Europe and considered at the experimental site 2 in Orléans (kyr = thousand years).**

### 2.3 Numerical model development

Transient conductive heat transfer was simulated in one dimension to reproduce the temperature corrected for glaciation effects using the finite element program COMSOL Multiphysics solving equation 2. The finite element method had been used in the past to solve the 1D heat transfer equation (Aziz and Monk, 1989; Dabral *et al.*, 2011). Only conductive heat transfer in solids is considered to reproduce temperature profiles measured in boreholes and simulate the transient thermal perturbation induced to the ground by the increase of temperature at surface due to climate warming. The heat transfer in solids module appears most appropriate since the problem to solve is dominantly affected by heat diffusion:

$$\frac{\partial}{\partial x} \left( \lambda \frac{\partial T}{\partial x} \right) = \rho c \frac{\partial T}{\partial t} \quad (2)$$

where  $\lambda$  ( $\text{W m}^{-1} \text{K}^{-1}$ ) is the thermal conductivity,  $\rho$  ( $\text{kg m}^{-3}$ ) is the density and  $c$  ( $\text{J kg}^{-1} \text{K}^{-1}$ ) is the heat capacity. The thermal properties of the subsurface of each layer were assumed to be uniform and constant through time. The heat generation rate due to the decay of radioactive elements in the subsurface was neglected since the simulated domain is relatively shallow (Raymond *et al.*, 2016).

The bottom boundary condition was a constant heat flow, which represents the Earth natural heat flow towards the surface. The model had a length of 700 m in the vertical direction to minimize the effect of the bottom boundary condition that can influence the propagation of temperature changes at the surface if located too close to the surface. A historical surface temperature varying with time was applied at the top of the domain as boundary condition taking into account the recent climate warming of the last century. Air temperature measurements at the Jean Lesage airport from 1943 to 2016 and available from the web site of Environment Canada (<http://climate.weather.gc.ca/>) were used at experimental site 1 in Quebec City to define the magnitude of historical temperature changes (Figure 5). Three sources of surface temperature were used at experimental site 2 in Orléans (Figure 5). Air and land surface temperature measured at the weather station of the experimental geothermal platform from January to May 2017 were used for the last period with data available at <http://plateforme-geothermie.brgm.fr/fr/suivi/METEO>. Air temperature measurements from 1996 to 2016 at a weather station in Tours, located 118 km from Orléans, were used for the middle period with data available at <https://donneespubliques.meteofrance.fr> (station ID: 07240). In the absence of temperature data near Orléans before 1996, the mean air temperature in France was used from 1901 to 1996 for the initial period with data available at: <http://sdwebx.worldbank.org/climateportal/>.



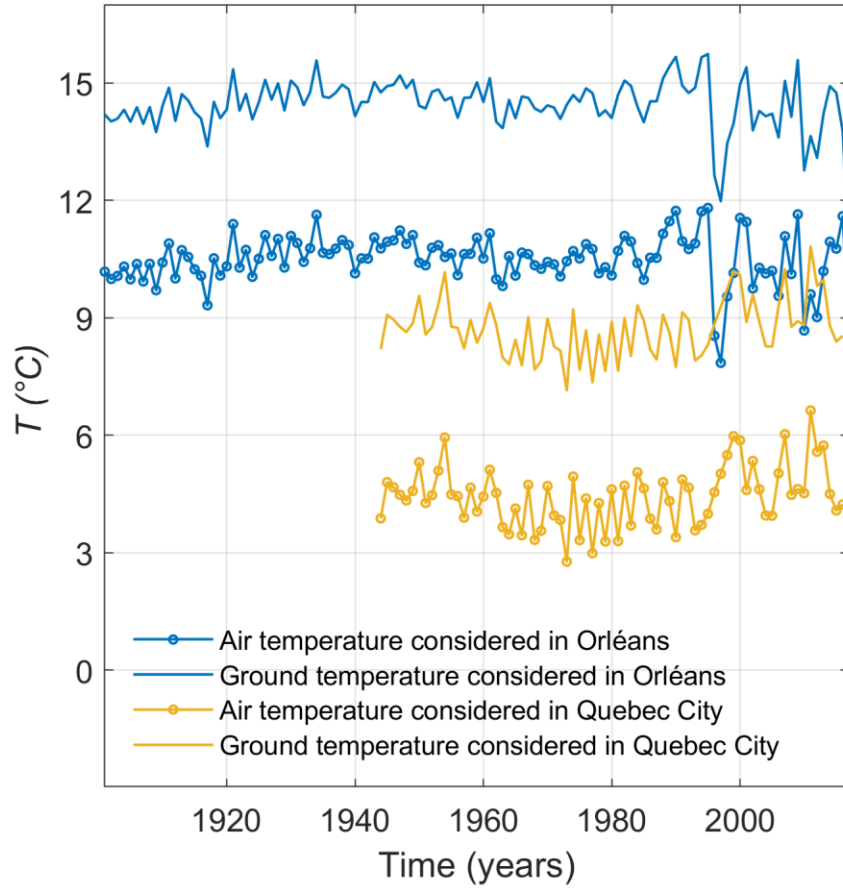


**Figure 5. Historic air and ground temperature variations considered in Quebec City (yellow lines) and Orléans (blue lines).**

Air temperature was converted to ground surface temperature (Figure 4), defining the magnitude of the temperature changes at the top boundary of the model. The conversion of air to ground temperature was made using an empirical relationship developed by Ouzzane *et al.* (2015) defined as:

$$T_g = 17.898 + 0.951T_{amb} \quad (3)$$

where  $T_g$  (K) is the ground surface temperature and  $T_{amb}$  (K) is the ambient air temperature. The relation is based on the fact that among the parameters controlling the ground surface temperature (ambient temperature, sky temperature, wind velocity and solar radiation), the ambient temperature is the dominant parameter, therefore  $T_g$  can be correlated as a function of the ambient temperature only (Ouzzane *et al.*, 2015). The use of this empirical relationship resulted in an estimated ground surface temperature that is approximately 4 K higher than the air temperature (Figure 5). The resulting temperature

evolution was used to define the relative temperature changes at the model upper boundary, adjusting the historic temperature curve to begin at an initial temperature characteristic of the measured temperature profile.

The exact value of the initial temperature for the boundary condition at the surface ( $T_s$ ) was inferred from the undisturbed geothermal gradient measured at the bottom of the boreholes (last 40 m), which are less influenced by the ground surface temperature variations than the temperature in the upper section of the GHEs. These temperatures were extrapolated upward according to the equilibrium geothermal gradient to set the initial temperature at the surface according to (Raymond *et al.*, 2016):

$$T_s = \frac{-b}{m} \quad (4)$$

where  $b$  and  $m$  are the y-intercept and the slope of the graphic of temperature at depth in the last 40 m of the boreholes. The initial temperature condition needed to run the transient simulations was then calculated according to the basal heat flow  $q$  ( $\text{W m}^{-2}$ ) for temperature distribution to follow the equilibrium geothermal gradient:

$$T_i = T_s + \left( \frac{q}{\lambda_s} \right) \cdot z \quad (5)$$

where  $\lambda_s$  ( $\text{W m}^{-1} \text{K}^{-1}$ ) is the subsurface thermal conductivity and  $z$  (m) is the depth. The basal heat flow was optimized and therefore changed every simulation such that the initial temperature distribution was recalculated automatically with equation 5 every simulation.

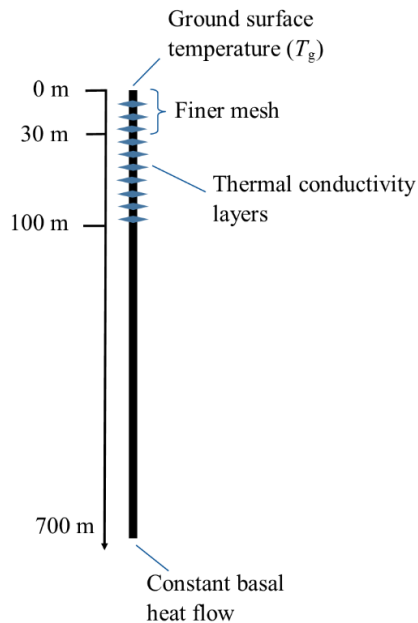


**Figure 6. Simulation domain and boundary condition.**

The transient simulations to reproduce the observed temperature profiles were carried out for a duration of 72 and 116 years for Quebec City and Orléans experiment sites, respectively, with monthly time steps. The simulation times were equal to the available historic air temperature data.

A sensitivity analysis was carried out to define the depth at which the basal heat flow should be imposed and the mesh resolution to make sure the obtained temperature solution is reliable. The position of the bottom heat flow boundary condition and the mesh resolution were gradually increased to verify the model independence with respect to the position of the bottom boundary and the mesh size.

A uniform coarse mesh was initially defined in all the domain, then the mesh was gradually refined using the predefined COMSOL meshes until achieve a constant temperature in a given depth to verify the model independency from the mesh resolution. This initial refinement did not allow to reproduce the upper part of the profile affected by the seasonal temperature variation. A finer mesh was needed in the first 30 m of the profile to achieve a reliable reproduction of the temperature profiles. However, this finer mesh was only applied in the upper part of the profile to keep the calculation time short.

The position of the bottom boundary condition was increased each 50 m, from 100 to 700 m depth until an insignificant relative difference between the simulated temperature

at a given depth was achieved. The thermal conductivity after 100 m is unknown. A sensitivity analysis varying the thermal conductivity in this last layer within the interval of thermal conductivity estimated in the TRT was made. The modification of the thermal conductivity results in a fluctuation of less than 10% in the simulated temperature and the inferred heat flow. Therefore, the average thermal conductivity estimated in the TRT (Figure 1) was assumed from 100 to 700 m depth.

Inverse numerical simulations to optimize the basal heat flow and reproduce the observed temperature were made once the model was proven to be independent of boundary location and mesh. The optimization module was chosen to perform inverse simulations and automatically infer the lower boundary condition of the model, which is the Earth heat flow (Figure 6). The least-squares function allowed comparing measured and observed temperature profiles and the function was minimized with the Coordinate search solver (Conn *et al.*, 2009). This solver was chosen because it provided a rapid method to find the minimum while aiming at improving the objective function along the coordinate directions. The step lengths are decreased or increased according to the values of the objective function (COMSOL AB, 2013). The Coordinate search solver stops iterating as soon as no improvement over the current best estimate can be made with steps of relative size larger than or equal to the optimality tolerance (COMSOL AB, 2013). The inverse modeling approach was validated for the heat conduction problem solved with steady-state simulations shown in Annex 1 to reproduce a temperature profile calculated analytically. The optimality tolerance of the solver for the two field cases presented in this work was defined at  $1 \times 10^{-6}$  and the maximum number of objective evaluation was set to 100. The convergence was achieved at 34 and 43 iterations in Quebec City and Orléans, respectively.

## 3 Results

### 3.1 Paleoclimate correction

The paleoclimate correction of the measured temperature profiles achieved for the glaciations resulted in an increase of the temperature at depth. Considering the last four glaciations and a temperature step of 5 K, the average temperature increase for the profile in Quebec City was 0.14 K, with a maximal increase of 0.31 K at the bottom of the profile (Figure 7a). The average temperature increase, for the profile measured in

Orléans, where the last five glaciations and a temperature step of 7 K were considered, was 0.31 K with a maximal value of 0.60 K at the bottom of the profile (Figure 7b). The corrected temperature was used for observations to reproduce with the numerical model.

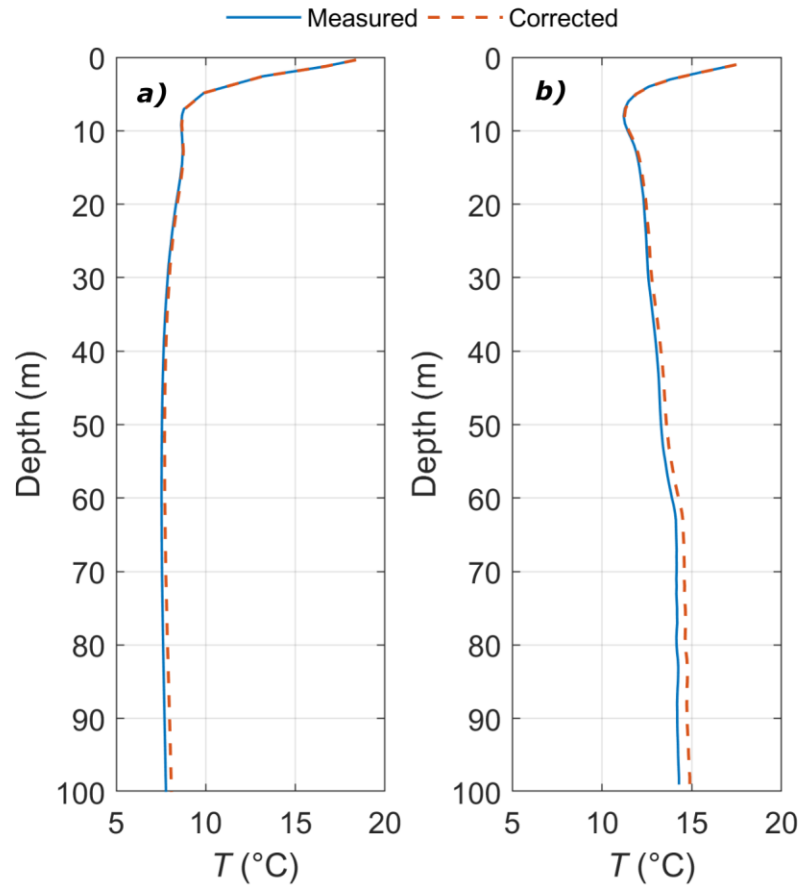


**Figure 7. Temperatures corrected for paleoclimate effects of the Quaternary glaciations for the sites a) in Quebec City and b) in Orléans.**

### 3.2 Numerical simulation

The sensitivity analysis indicated the mesh resolution and the model depth have an influence on the simulated temperature. A mesh with 60 and 140 elements was needed to achieve accurate simulations of the temperature profile with little temperature difference in between simulation cases for the models representing the experimental site in Quebec City and Orléans, respectively (Table 1). The bottom boundary was defined at 700 m depth in both cases to reduce its influence on the simulated temperature

(Table 1). Temperature extracted at 30 m depth is given to show the impact of the model mesh and bottom boundary position, evidencing the model independence.

**Table 1. Verification of the mesh independence and the bottom heat flow boundary position.**

Number of elements			
Site 1		Temperature at 30 m depth	Relative difference (%)
	53	8.5061	-
	58	8.4445	0.7293
	60	8.4445	0.0000
Site 2			
	71	12.4230	-
	90	12.9881	0.5651
	140	13.0961	0.1080
Bottom boundary location (m)			
Site 1			
	600	8.1266	-
	650	8.1260	0.0076
	700	8.1260	0.0000
Site 2			
	600	12.9666	-
	650	13.2534	2.1639
	700	13.0961	1.2009

An initial manual optimization of the heat flow was carried out, to reduce the heat flow range to optimize with the solver. Using the heat transfer module, a model to simulate transient heat conduction in solids was created. Heat flow values varying between 10 and 100 mW m<sup>-2</sup> were assigned to the bottom boundary condition to verify their impact on the difference between simulated and measured temperature, to reduce the possible heat flow range before proceeding to optimization.

The lower and upper bound for the heat flow optimization of the model representing the site in Quebec City were 10 and 40 mW m<sup>-2</sup>, respectively, while a range varying from 30 to 70 mW m<sup>-2</sup> was defined for the site in Orléans. Then, the least-squares function and the coordinate search method were used to optimize the heat flow bottom boundary condition and reproduce the measured temperature profile. The optimization started at the lowest heat flow value.

The least-square residuals for optimization of the heat flow at experimental site 1 decreased from 20 to 7.97 for the best fit scenario (Figure 8a), where the basal heat flow

was  $28.9 \text{ mW m}^{-2}$  (Figure 9). A heat flow of  $43.6 \text{ mW m}^{-2}$  was found for experimental site 2 (Figure 9), with a reduction of the least-square residuals from 515.43 to 27.87 (Figure 8b).

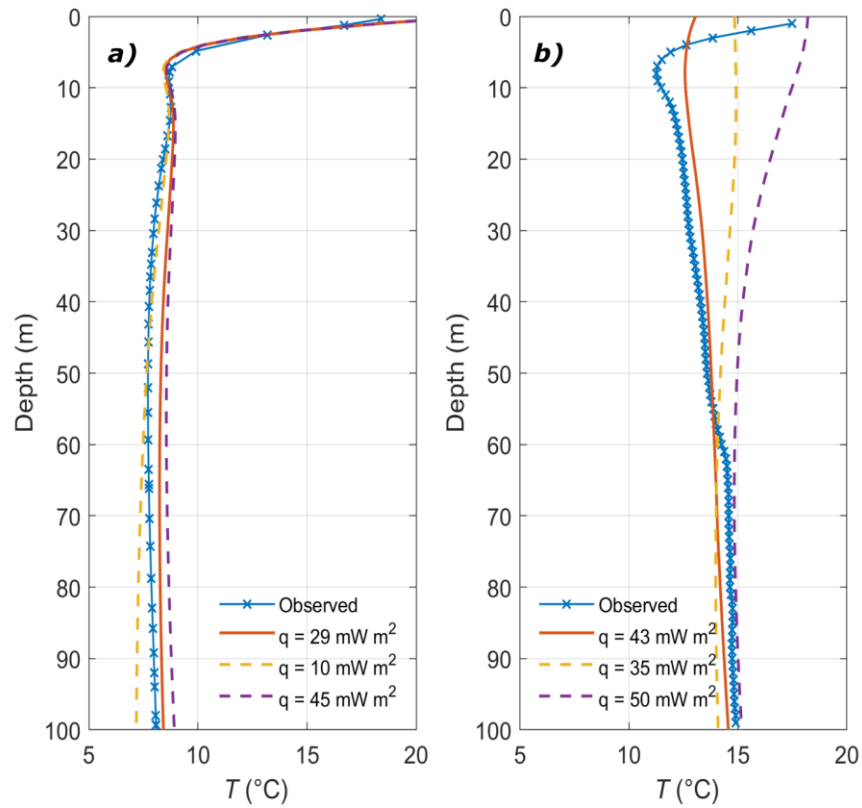


**Figure 8. Simulated temperature corresponding to the different heat flow at the bottom boundary for the sites a) in Quebec City and b) in Orléans. The continuous line corresponds to the optimized heat flow.**

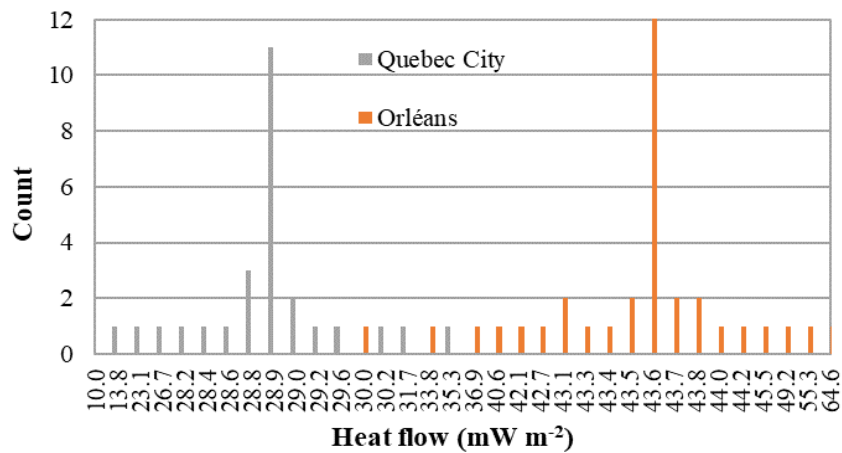


**Figure 9. The histogram of basal heat flow values tried by the coordinate search solver to find the solution that best reproduces temperature measurements for Quebec City (grey bars) and Orléans (orange bars).**

Equilibrium heat flow estimations in the study areas located in cities are not available. Heat flow map of the Quebec Province indicates a heat flow in the range of 30 to 40  $\text{mW m}^{-2}$  for the Quebec City area (Figure 10, Mareschal *et al.*, 2010). The heat flow estimated with the numerical simulations in Quebec City correspond to the lower value of this interval.

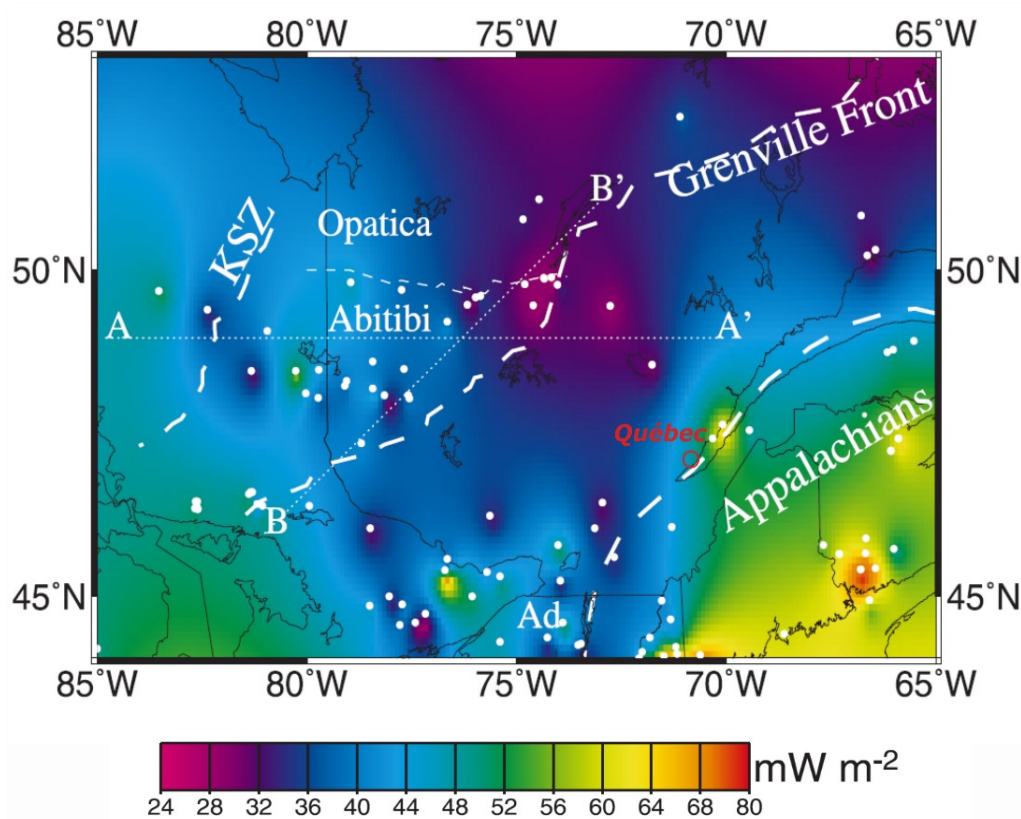


**Figure 10. Heat flow map of Eastern Canada. The white dots represent the sites where the heat flow has been evaluated with borehole measurements generally deeper than those used for TRT (modified from Mareschal *et al.*, 2000).**

A value varying from 100 to 110  $\text{mW m}^{-2}$  characterizes the Orléans site according to the heat flow map of France (Figure 11, SIG Mines France, 2007). The estimated heat flow in Orléans is lower than the reported value for the area. Nevertheless, the calculated value is a point estimation of the near-surface heat flow and the map provides estimations at the country scale, making comparison difficult.



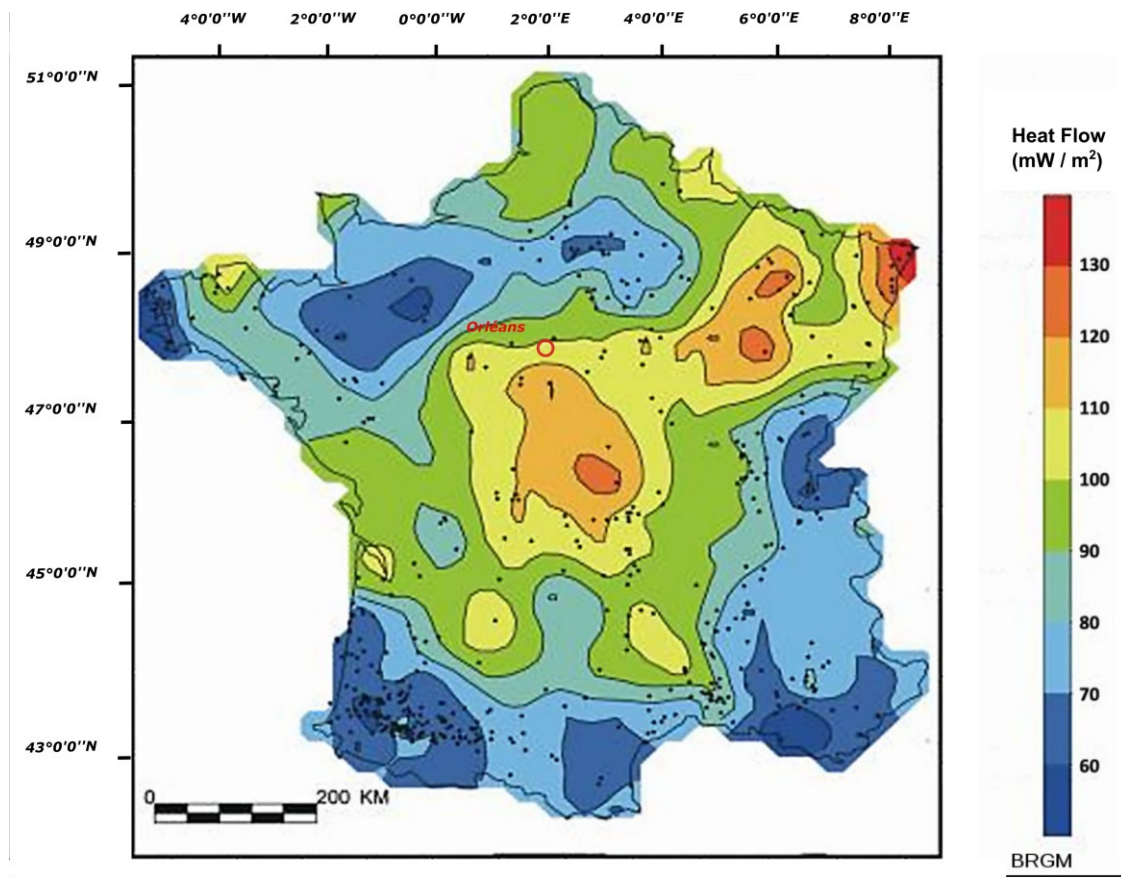


**Figure 11. Heat flow map of France. The black dots represent the sites where the heat flow has been evaluated with borehole measurements generally deeper than those used for TRT (modified from SIG Mines France, 2007).**

## 4 Discussion

A method, relying on thermal response tests (TRT) and undisturbed temperature profiles in ground heat exchangers was presented in this work, to extend the use of TRT for the evaluation of heat flow essential for deep geothermal resource assessment. The proposed analysis provides a preliminary estimation of the Earth heat flow in the near-surface with relatively shallow boreholes. A depth of approximately 100 m is typically not deep enough to infer the ground surface temperature history with inverse simulations of heat transfer to reproduce temperature measured in such a short borehole (Jessop, 1990). A borehole unaffected by paleoclimates in its deeper part is needed to infer both the site heat flow and temperature history in a single optimization sequence. A depth of more than 3000 m seems to be optimal to resolve the temperature rise after the glacial

period adequately. Nevertheless, undisturbed temperature logs that deep are rare (Hartmannv & Rath, 2005). In the circumstance of a shallow borehole, ground surface temperature can be evaluated from other paleoclimate studies with deeper boreholes and taken into account to correct the temperature measurement of shallower boreholes. A depth of about 300 to 500 m is suitable to derive a mean temperature for the last 1000 years (Hartmannv & Rath, 2005). The observed temperature profiles measured in the studied ground heat exchangers were corrected analytically according to the paleoclimate effects of the quaternary glaciations in North America and Europe with forward calculations since the boreholes analyzed were relatively short. Simulations to reproduce corrected and uncorrected temperature profiles were performed. Without paleoclimate correction for glaciations, the optimized heat flow in Quebec City decrease from 28.9 to 22.5 mW m<sup>-2</sup> and from 43.6 to 39.7 mW m<sup>-2</sup> in Orléans. The surface temperature perturbation due to the recent climate warming was treated afterward with numerical simulations.

In fact, the undisturbed temperature profiles reported for this study were reproduced with an inverse numerical model simulating conductive heat transfer to estimate the site heat flow through the optimization of the bottom boundary condition. The historic ground surface temperature affected by the recent climate warming was used to define the magnitude of temperature changes at the model upper boundary. Data recorded at weather stations constrained simulations to cope with the shallow depth of the 100 m boreholes that is not sufficient to accurately infer the ground surface temperature history. The historic surface temperatures near the experimental site in Orléans were not available before 1996. Therefore, surface temperature history of France was used from 1901 to 1996. This value may not represent the exact temperature variation at the study area and can explain the poor temperature match near the surface. A more accurate estimation of the heat flow at this site would require a better definition of the upper boundary condition. Nevertheless, the heat flow estimated at both sites is small and the potential for deep geothermal resources is low.

The approach presented in this work can be used for the preliminary evaluation of heat flow with TRT and ground heat exchangers, aiming at the exploration of deep geothermal resources of urban areas. This can reduce exploration risks, where deep wells are sparse and geothermal heat pump system common, which is the case of cities. Deep boreholes suitable for heat flow assessment are rarely drilled in populated towns,

although energy needs and potential to develop geothermal direct use can be significant due to the population density.

## 5 Conclusions

An inverse numerical model based on inferred thermal conductivity profiles from thermal response test and temperature profiles measured in ground heat exchangers has been developed to estimate terrestrial heat flux near the surface. This methodology helps to fill the lack of heat flux observations in urban areas. It could be combined in future work with heat flux observations on deep boreholes, outside but close to cities, in order to define the potential of deep geothermal resources of urban areas where the demand for heat is high. The direct use of geothermal resources for heating purposes is generally restricted to one or two kilometers of the pumping and injection wells, a location which must coincide with adjacent energy markets. The analysis of TRTs and temperature profiles is a tangible way to better define the heat flux and geothermal resources of these urban energy markets.

Further work can now be envisioned to collect TRT dataset from private companies and use the approach described in this paper to better define heat flow distribution. For example, more than 100 TRTs have been inventoried in the St. Lawrence Lowlands hosting populated cities of Montreal and Québec (Bédard *et al.*, 2018), while only three deep wells are available for this region to evaluate heat flow (Fou, 1969; Saull *et al.*, 1962). In fact, the Earth heat flow could be estimated where temperature profiles have been measured in ground heat exchangers before doing TRT to improve current geothermal resources assessment based on bottom-hole temperature that is not in equilibrium with the host rock (Bédard *et al.*, 2012; Majorowicz and Minea, 2012). In the absence of equilibrium temperature profiles in deep boreholes, these authors have used public bottom hole temperature records, which can contain mistakes and can be difficult to accurately correct for drilling disturbance, resulting in significant uncertainty about the geothermal potential (Bédard *et al.*, 2014). Analysis of equilibrium temperature in ground heat exchangers, although shallow, can help reduce this uncertainty to eventually justify the drilling of a deep borehole for equilibrium temperature profiling. Such invasive exploration work that is more accurate, but has a greater environmental impact, needs to be better justified because of its important cost.

## Acknowledgments

The Natural Sciences and Engineering Research Council of Canada is acknowledged for funding this research. The French geological survey (Bureau de Recherches Géologiques et Minières) in Orléans, France, is acknowledged for making available the experimental geothermal test facility in Orléans to conduct a part of this research.

The IGCP, UNESCO, and IUGS are finally acknowledged since this work is part of the project “IGCP 636-Unifying international research forces to unlock and strengthen geothermal exploitation of the Americas and Europe”, currently funded by UNESCO (United Nations Educational, Scientific and Cultural Organization) and IUGS (International Union of Geological Sciences) within the International Geoscience Programme (IGCP).

## References

Allis RG. (1978). The effect of Pleistocene climatic variations on the geothermal regime in Ontario: a reassessment. *Canadian Journal of Earth Sciences* 16(7):1517-1517. doi:10.1139/e79-137.

Aziz AK, Monk P. (1989). Continuous finite elements in space and time for the heat equation. *Mathematics of Computation* 52(186):255-74. Bédard K, Comeau FA, Raymond J, Gloaguen E, Comeau G, Millet E, Foy S. (2018). Cartographie de la conductivité thermique des Basses-Terres du Saint-Laurent. Rapport de recherche (R1789). INRS, Centre Eau Terre Environnement, Québec.

Bédard K, Comeau FA, Raymond J, Malo M, Nasr M. (2017). Geothermal Characterization of the St. Lawrence Lowlands Sedimentary Basin, Québec, Canada. *Natural Resources Research* 10.1007/s11053-017-9363-2. doi:10.1007/s11053-017-9363-2.

Bédard K, Raymond J, Malo M, Konstantinovskaya E, Minea V. (2014). St. Lawrence Lowlands bottom-hole temperature: various correction methods. *GRC Trans.* 38, 351–355.

463 Bédard K, Comeau FA, Malo M. (2012). Capacité effective de stockage géologique du  
 464 CO<sub>2</sub> dans le bassin des Basses-Terres du Saint-Laurent (No. INRSCO2–2012–  
 465 V3.1). Institut national de la recherche scientifique - Centre Eau Terre  
 466 Environnement, Québec, Canada.

467 Beck AE. (1977). Climatically perturbed temperature gradients and their effect on  
 468 regional and continental heat-flow means. *Tectonophysics*, 41(1), 17-39.  
 469 doi:[https://doi.org/10.1016/0040-1951\(77\)90178-0](https://doi.org/10.1016/0040-1951(77)90178-0)

470 Bodri L, Cermak V. (2007). CHAPTER 2 - Climate Change and Subsurface  
 471 Temperature. in *Borehole Climatology* (pp 37-173). Oxford: Elsevier.

472 COMSOL AB. (2016). COMSOL Multiphysics Reference Manual. Stockholm.

473 COMSOL AB. (2013). Optimization Module User's Guide, version 4.4. Stockholm.

474 Conn AR, Scheinberg K. Vicente LN. (2009). Introduction to derivative-free optimization  
 475 (Vol. 8). Philadelphia: Siam.

476 Dabral V, Kapoor S, Dhawan S. (2011). Numerical Simulation of one dimensional Heat  
 477 Equation: B-Spline Finite Element Method. *Indian Journal of Computer Science  
 478 and Engineering (IJCSE)* Vol. 2:222-35. Davies JH (2013) Global map of solid  
 479 Earth surface heat flow. *Geochemistry, Geophysics, Geosystems* 14(10):4608-  
 480 4622. doi:10.1002/ggge.20271.

481 Fou JTK. (1969). Thermal conductivity and heat flow at St. Jérôme, Quebec (M.Sc.  
 482 Thesis). McGill University, Montreal, Canada.

483 Golovanova IV, Sal'manova RY, Tagirova CD. (2014). Method for deep temperature  
 484 estimation with regard to the paleoclimate influence on heat flow. *Russian Geology  
 485 and Geophysics* 55(9):1130-1137. doi:<https://doi.org/10.1016/j.rgg.2014.08.008>.

486 Hartmann A, & Rath V. (2005). Uncertainties and shortcomings of ground surface  
 487 temperature histories derived from inversion of temperature logs. *Journal of  
 488 Geophysics and Engineering*, 2(4), 299.

489 Jessop AM. (1990). Chapter 3 - Analysis and Correction of Heat Flow on Land. *Thermal  
 490 Geophysics* (pp 57-85). Vol.17. Amsterdam: Elsevier.

491 Majorowicz JA, Minea V. (2012). Geothermal energy potential in the St-Lawrence River  
 492 area, Québec. *Geothermics* 43, 25–36.  
 493 <https://doi.org/10.1016/j.geothermics.2012.03.002>

494 Majorowicz J, Wybraniec S. (2011). New terrestrial heat flow map of Europe after  
 495 regional paleoclimatic correction application. *International Journal of Earth*  
 496 *Sciences* 100(4):881-887. doi:10.1007/s00531-010-0526-1.

497 Majorowicz J, Šafanda J. (2008). Heat flow variation with depth in Poland: evidence from  
 498 equilibrium temperature logs in 2.9-km-deep well Torun-1. *International Journal of*  
 499 *Earth Sciences* 97(2):307-315. doi:10.1007/s00531-007-0210-2.

500 Mareschal JC, Jaupart C. (2004). Variations of surface heat flow and lithospheric  
 501 thermal structure beneath the North American craton. *Earth and Planetary Science*  
 502 *Letters* 223(1):65-77. doi: 10.1016/j.epsl.2004.04.002.

503 Mareschal JC, Jaupart C, Gariépy C, Cheng LZ, Guillou-Frottier L, Bienfait G, Lapointe  
 504 R. (2000). Heat flow and deep thermal structure near the southeastern edge of the  
 505 Canadian Shield. *Canadian Journal of Earth Sciences* 37(2-3):399-414. doi:  
 506 10.1139/e98-106.

507 Ouzzane M, Eslami-Nejad P, Badache M, Aidoun Z. (2015). New correlations for the  
 508 prediction of the undisturbed ground temperature. *Geothermics* 53:379-384.  
 509 doi:10.1016/j.geothermics.2014.08.001.

510 Raymond J, Lamarche L, Malo M. (2016). Extending thermal response test assessments  
 511 with inverse numerical modeling of temperature profiles measured in ground heat  
 512 exchangers. *Renewable Energy* 99:614-621. doi:10.1016/j.renene.2016.07.005.

513 Raymond J, Lamarche L. (2014). Development and numerical validation of a novel  
 514 thermal response test with a low power source. *Geothermics* 51:434-444.  
 515 doi:10.1016/j.geothermics.2014.02.004.

516 Sanner B, Hellström G, Spitler J, Gehlin S. (2013). More than 15 years of mobile  
 517 Thermal Response Test—a summary of experiences and prospects. *European*  
 518 *Geothermal Congress*, Pisa.

- 519 Sass JH, Beardsmore G. (2011). Heat Flow Measurements, Continental. *Encyclopedia*  
 520 *of Solid Earth Geophysics* (pp 569-573). Dordrecht: Springer. doi:10.1007/978-90-  
 521 481-8702-7\_72.
- 522 SIG Mines France. (2007). Données thermiques (flux de chaleur et température).  
 523 Bureau de recherches géologiques et minières, Orléans.  
 524 [http://sigminesfrance.brgm.fr/geophy\\_flux.asp](http://sigminesfrance.brgm.fr/geophy_flux.asp). (Consulté le 15 mai 2018).
- 525 Saull VA, Clark TH, Doig RP, Butler RB. (1962). Terrestrial Heat Flow in the St.  
 526 Lawrence Lowland of Québec. Can. Min. Metall. Bull. 65, 63–66.
- 527 Velez-Marquez MI, Raymond J, Blessent D, Philippe M, Simon N, Bour O, Lamarche L.  
 528 (2018). Distributed thermal response tests using a heating cable and fiber optic  
 529 temperature sensing. *Energies* 11(11), 3059; doi:10.3390/en11113059..
- 530 Westaway R, Younger PL. (2013). Accounting for paleoclimate and topography: A  
 531 rigorous approach to correction of the British geothermal dataset.  
 532 *Geothermics* 48:31-51. doi:10.1016/j.geothermics.2013.03.009.

## 533 Annex 1: Model validation

534 A validation of the inverse and conductive heat transfer modeling approach was  
 535 performed before analyzing the data set presented in this work. The results of the model  
 536 validation is given below.

537 The modeling approach was verified with a steady-state heat conduction simulation to  
 538 reproduce a synthetic temperature profile calculated according to Fourier's law (Eq. 6):

$$539 \quad q = -\lambda \frac{dT}{dz} \quad (6)$$

540 where  $q$  (W m<sup>-2</sup>) is the heat flow,  $\lambda$  (W m<sup>-1</sup> K<sup>-1</sup>) is the thermal conductivity,  $T$  (K) is the  
 541 temperature and  $z$  (m) is the depth. The synthetic temperature profile was calculated  
 542 analytically defining a constant subsurface thermal conductivity of 2 W m<sup>-1</sup> K<sup>-1</sup>, a basal  
 543 heat flow equal to 0.050 Wm<sup>-2</sup> and a surface temperature of 8 °C (Figure 12).

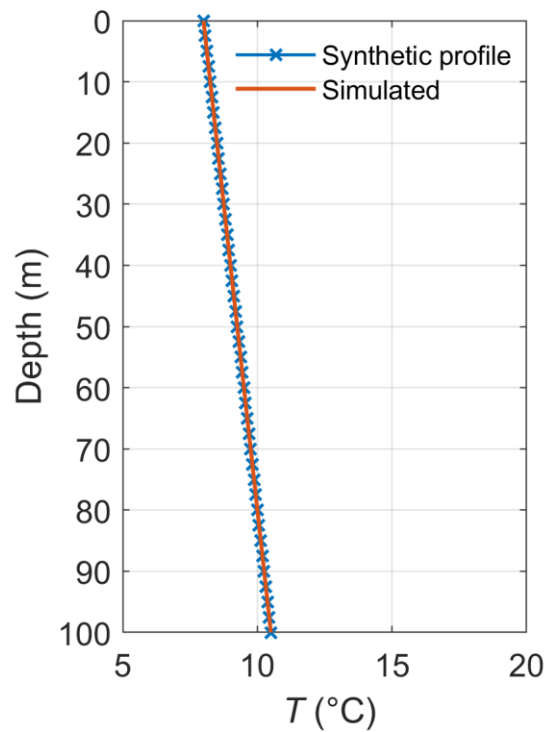


**Figure 112. Temperature profile simulated numerically reproducing the synthetic temperature profile determined analytically.**

The subsurface thermal conductivity used in the COMSOL finite element model was set to the same value of  $2 \text{ W m}^{-1} \text{ K}^{-1}$  and constant surface temperature equal to  $8 \text{ }^{\circ}\text{C}$  was defined as the upper boundary condition. The optimization module was used to find with the Coordinate search solver the heat flow at the bottom boundary and reproduce the synthetic temperature profile (Figure 12). The least square residual computed by comparing temperature profiles defined numerically and analytically decreased from  $254.83$  to  $8.56 \times 10^{-4}$ , converging toward the expected heat flow value of  $0.050 \text{ mWm}^{-2}$  (Figure 13), which validated the inverse modeling approach.



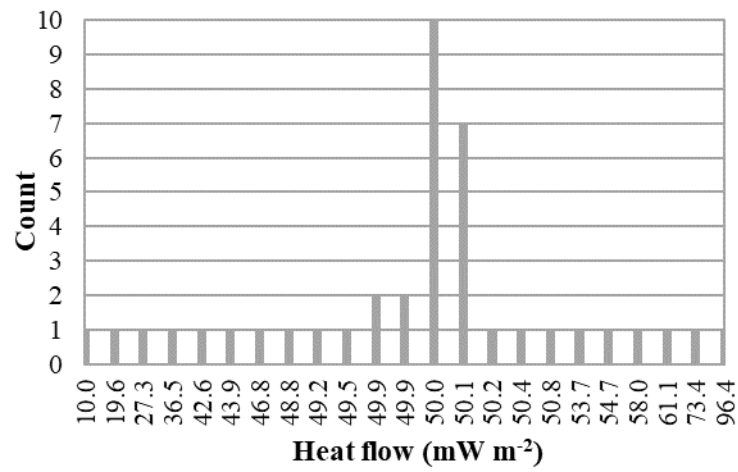


**Figure 113. Histogram of basal heat flow values tried by the coordinate search solver to find the solution that best reproduces the synthetic temperature profile determined analytically.**